Available online at www.sciencedirect.com
SCIENCE DIRECT®

Journal of the European Ceramic Society 23 (2003) 1499–1508

www.elsevier.com/locate/jeurceramsoc

Microstructure of SiC deposited from methyltrichlorosilane

Boris Reznik[a], Dagmar Gerthsen[a], Weigang Zhang[b], Klaus J. Hüttinger[b,*]

[a]*Laboratorium für Elektronenmikroskopie, Universität Karlsruhe, Kaiserstr. 12, D-76128 Karlsruhe, Germany*
[b]*Institut für Chemische Technik, Universität Karlsruhe, Kaiserstr. 12, D-76128 Karlsruhe, Germany*

Received 1 March 2002; received in revised form 12 September 2002; accepted 22 September 2002

Abstract

Micro- and nanostructure of silicon carbide deposited at a pressure of 90 kPa and temperatures of 900, 1000 and 1100 °C from a methyltrichlorosilane/hydrogen mixture of 1:4 were investigated by TEM, HRTEM and energy-filtering diffraction (EFD); the chlorine content was studied by PEELS. The deposit at 1100 °C is characterized by highly textured, heavily faulted columnar β-SiC with some α-SiC, which should result from a twinning transformation. At the lower temperatures of 1000 and 900 °C Si is co-deposited. Simultaneously, smaller sized and less perfect nanocrystals of β-SiC are formed. At 1000 °C the nanocrystals of β-SiC and Si are separated by a weakly crystallized interphase; at 900 °C the nanocrystals are randomly dispersed in a disordered matrix phase. Chlorine is detected in all samples. Fringe patterns of some areas of the matrix phase at 900 °C show an interplanar distance of 0.44 ± 0.02 nm which corresponds to that of polychlorosilane, $[SiCl_2]_n$. This correspondence suggests condensation of polychloro- and probably also of polycarbochlorosilanes during the deposition process at low temperatures.

Keywords: Composites; Electron microscopy; Engine components; SiC

1. Introduction

X-ray diffraction (XRD), scanning electron microscopy (SEM), conventional and high resolution transmission electron microscopy (TEM, HRTEM) as well as Raman spectroscopy were used in literature for structural analysis of SiC deposited by chemical vapor deposition (CVD) (Refs. 1–8, among others). Some general tendencies may be derived from these studies: Columnar stoichiometric SiC is preferentially deposited at high temperatures; the influence of pressure is small.[1,2] Co-deposition of Si is favored at low temperatures and enhanced by increasing pressure. Simultaneously, the crystallite sizes decrease.[2] These tendencies are attributed to different rate limiting steps, mass transfer at high temperatures and surface reactions at low pressures.[2,9,10] Limitation of surface reactions leading to stoichiometric SiC is ascribed to Si–Cl and C–H bond cleavages followed by HCl elimination. Co-deposition of Si at low temperatures is explained by a reduction of the Si–Cl bond with H_2. Small species, in particular $SiCl_2$, $SiCl_3$ and CH_3, are generally postulated to form both, SiC and Si.[9–11] SiC is a highly complex material existing in many polytypic forms,[12] which are based on various stacking sequences of a basic structural unit, a 2-layer planar unit of Si and C in tetrahedral coordination. 3C SiC is the only polytype with cubic symmetry; it also known as β-SiC with a lattice constant $a = 0.4358$ nm. When heated to high temperatures, β-SiC transforms to a mixture of hexagonal (6H) and rhombohedral (15R) polytypes; these polytypes are collectively known as α-SiC and have lattice constant parameters of $a = 0.3082$ nm and $c = 1.5117$ nm [13].

The chemistry of chemical vapor deposition of SiC from small molecules and radicals as postulated in literature[9,14,15] was questioned in recent studies of CVD of SiC from methyltrichlorosilane (MTS) and hydrogen.[16–18] In these studies deposition rates as well as composition of the deposits were determined as a function of substrate length at temperatures from 800 to 1100 °C using substrates with different surface area/volume ratios, (A/V), for the first time. The gas phase composition was determined as a function of residence time.

* Corresponding author. Tel.: +49-721-608-2114; fax: +49-721-608-4820.
E-mail address: huettinger@ict.uni-karlsruhe.de (K.J. Hüttinger).

0955-2219/03/$ - see front matter © 2003 Elsevier Science Ltd. All rights reserved.
PII: S0955-2219(02)00364-3

Quantitative X-ray diffraction and on line gas chromatography were used to analyze the composition of the deposits and the gas phase, respectively.

X-ray diffraction analysis shows deposition of stoichiometric SiC at 1100 °C and a possible co-deposition of free silicon at decreasing temperature, which is in agreement with earlier results.[2,3] Co-deposition was additionally found to depend on the reactor length and especially on the (A/V) ratio (Fig. 1), a parameter which was shown in earlier studies to strongly influence deposition chemistry (Refs. 19, 20 among others).

Fig. 1 shows deposition rates as a function of temperature obtained at surface area/volume ratios, [A/V], of 0.78 (a) and 3.55 mm^{-1} (b) with a MTS/H_2 mixture of 1:4. The results with the lower [A/V] ratio of 0.78 mm^{-1}, which is still higher than those used by other authors, are important because co-deposition of Si is favored. The most upper curve (■) represents the total deposition rate, the curves below the individual deposition rates of SiC (◇) and Si (○). Temperature selective, strong depositions of SiC as well as of Si at about 900 and 1025 °C are ascribed to a preformation of higher carbochloro- and chlorosilanes in the gas phase reactions.[17,18] Such a deposition process strongly deviates from earlier models and should have a direct impact on the growth features of the deposits. At the higher (A/V) ratio of 3.55 mm^{-1} formation of higher carbochloro- and chlorosilanes is limited leading to nearly stoichiometric SiC even at lower temperatures. This may be the reason for deposition of stoichiometric SiC during infiltration of fiber preforms exhibiting still higher (A/V) ratios.[1]

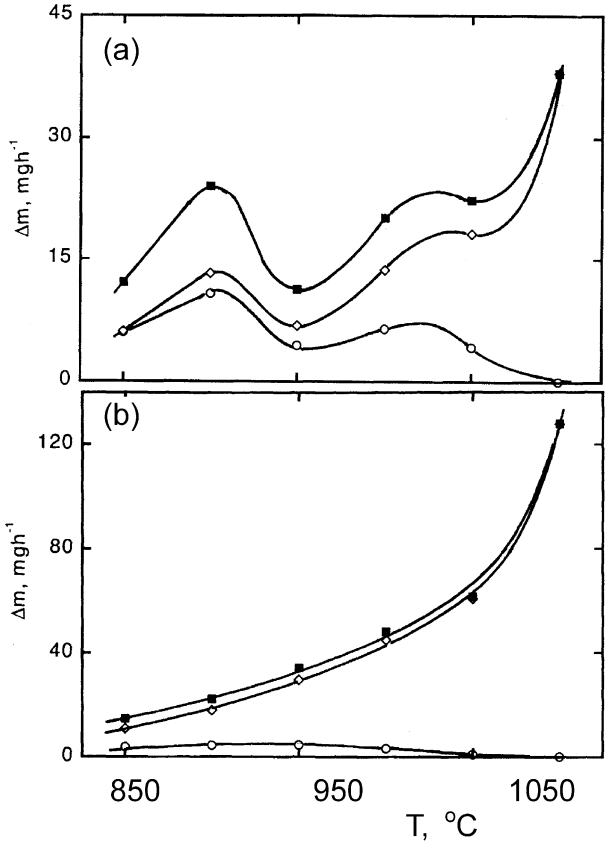

Fig. 1. Deposition rates of (◇) SiC, (○) Si and (■) the sum of both as a function of temperature at different substrates (A/V) ratios: (a) 0.78 mm^{-1} and (b) 3.55 mm^{-1}.

The present paper is concerned with detailed structural analyses of the deposits to correlate growth features with conclusions drawn from the proposed model, which postulates that larger carbochlorosilanes and chlorosilanes are decisive intermediates of the deposition of SiC and Si, respectively.[17,18] Samples deposited at 900, 1000 and 1100 °C at a (A/V) ratio of 0.78 mm^{-1} are investigated. TEM, HRTEM and energy-filtering diffraction (EFD) are used for structural analyses. The existence of chlorine and oxygen[2,3] is studied with parallel electron-energy-loss spectroscopy (PEELS), additionally.

2. Experimental

2.1. Chemical vapor deposition

The samples investigated correspond to those used for X-ray diffraction analysis.[17] They are deposited from a MTS/H_2 mixture of 1:4 on a silicon dioxide coated cordierite substrate at a (A/V) ratio of 0.78 mm^{-1}, temperatures of 900, 1000 and 1100 °C and a residence time of 0.9 s (corresponding to a substrate length of 38 mm).[16] The sample deposited at 1000 °C was additionally heat treated at 1100 °C for 40 h in flowing pure argon.

2.2. Transmission electron microscopy

For the TEM specimen preparation, slices with a thickness of 200 mm were cut from the substrate and further reduced in thickness by mechanical grinding and polishing to 80 μm. Typically, two argon guns operating at 1 kV, a current of 1 mA under an angle of 4° were used for the final etching of the sample from both sides. The powder-like material was placed on a holey carbon supporting film and studied using conventional TEM and HRTEM. The HRTEM studies were carried out using a Philips CM 200 FEG/ST electron microscope operated at 200 kV. The instrument is characterized by a Scherzer resolution of 0.24 nm and an information limit of 0.15 nm. The 'analySIS' software package (Soft-Imaging Software GmbH, Hammer Strasse 89, D-48153 Münster, Germany) was used for the fast fourier transformation (FFT) of HRTEM images.

2.3. Electron-energy-loss spectroscopy and energy-filtering diffraction

Chlorine and oxygen were analyzed by PEELS. Oxygen was not detected in any of the samples, chlorine was

analyzed by the Cl–$L_{2,3}$ absorption edge. The PEELS analyses combined with EFD were carried out in a LEO EM 912 Omega transmission electron microscope at an electron energy of 120 keV; this microscope is equipped with an Omega electron-energy spectrometer which is integrated into the projection lens system. The PEELS studies were performed on a 18 nm spot with a collection semiangle β of about 5 mrad. The spectra were taken with a 1024 × 1024 pixel charge-coupled-device (CCD) camera with an acquisition time of typically 10 ms. After collecting the spectra and normalizing, the background was stripped using a power low function procedure ("analySIS" software package). The limit for chlorine detection in this procedure is about 0.1%.[21]

3. Results

Results obtained with the sample deposited at 1100 °C are presented in Fig. 2. Fig. 2(a) shows a TEM image of heavily faulted columnar crystallites of β-SiC. The average size of a single crystal is about 150 nm. Faulted lamellae are oriented parallel to the (111) plane and the substrate surface according to the selected area electron diffraction (SAED). The corresponding SAED pattern (inset) contains reflections of a few superimposed columnar crystallites. The orthogonal axis of the diffraction pattern viewing perpendicular to the image plane is very close to the (110)-zone axis. The indexing of the diffraction pattern suggests highly textured SiC deposited with <111> direction oriented perpendicular to the substrate surface.

A HRTEM image taken from a thin crystallite is displayed in Fig. 2(b). FFT patterns [insets in Fig. 2(b)] from different parts of the TEM image show a slightly disorientation of about 5–10° between two parts of the crystallite. The FFT pattern taken from the upper left part (white dashed area) shows a set of strong reflections of β-SiC and a set of weak reflections of α-SiC.

The FFT pattern taken from the central part (inset right upper corner) corresponds to the (110) β-SiC zone axis slightly rotated with respect to the pattern in the upper left part. The relationship between the two orientations is (0001) α-SiC // (110) β-SiC.

Results obtained with the sample deposited at 1000 °C are presented in Fig. 3. Fig. 3(a) shows an overview image of the sample. On a nanoscale the material is rather homogeneous, but some inclusions may be observed (white circle). A corresponding diffraction pattern [Fig. 3(b)] shows diffuse Debye–Scherrer rings. The first three intensive rings correspond to diffractions from the (111), (220) and (311) of β-Si planes. Sharp Si reflections [arrows in Fig. 3(b)] are also observed. The (111) SiC dark-field image [Fig. 3(c)] demonstrates a rather homogeneous distribution of β-SiC crystallites with sizes ranging from 0.7 to 5 nm. Single crystallites with an average size of about 5 nm are shown in Fig. 3(d). Fig. 3(e) represents a HRTEM image of the area marked by a white circle in Fig. 3(a). It shows a relatively large Si crystallite and several lamellar β-SiC crystallites. These crystallites are separated by a less ordered interphase.

Results obtained with the same sample after heat treatment at 1100 °C are displayed in Fig. 4. Fig. 4(a) shows an overview micrograph indicating some recrystallization as compared to Fig. 3(a). A set of sharp rings corresponding to β-SiC and Si can be recognized from the diffraction pattern shown in Fig. 4(b). The dark-field images [Fig. 4(d) and (c)] were obtained by selecting a part of the β-SiC (111) and Si (111) rings with the aid of the objective aperture. They demonstrate that β-SiC seems to be the dominant phase in this sample. The crystallite sizes of β-SiC and Si are in the range from 10 to 30 nm which are much larger than those before heat treatment [Fig. 3(d) and (e)]. A Si crystallite with twins can be recognized to the left from the center of Fig. 4(e). The inter-phase between this crystallite and the adjacent matrix containing SiC crystallites shows a lower contrast as compared to the Si crystallites and the SiC matrix, as already observed in the sample before heat treatment [Fig. 3(e)]. A heat treatment at 1100 °C is obviously not sufficient to achieve a complete recrystallization of the matrix.

Results obtained with the sample deposited at 900 °C are presented in Figs. 5–7. The low contrast bright-field image [Fig. 5(a)] and the corresponding set of diffuse reflections [Fig. 5(b)] suggest a mixture of β-SiC and Si crystallites which are still less ordered as compared to those at 1000 °C. The distribution is demonstrated by dark-field images of β-SiC [Fig. 5(d)] and Si [Fig. 5(c)]. β-SiC and Si are homogeneously dispersed. A random distribution of β-SiC and Si crystallites is demonstrated by HRTEM [Fig. 6(a)]. The area marked by the white square containing a β-SiC and a Si crystallite was chosen for a Fourier image analysis. The corresponding FFT pattern [Fig. 6(b)] shows two spatial frequencies (marked as 1-1′ and 2-2′) which were selected for inverse Fourier transformation. The resulting images show a tilted boundary between two marked crystallites [Fig. 6(c) and (d)]. The size of the crystallites ranges up to 20 nm, only.

Fig. 7 presents results obtained with a powdered sample prepared from the same deposit. Fig. 7(a) shows a HRTEM image. The FFT pattern [Fig. 7(b)] taken from the dashed square area displays two spatial frequencies marked as 1-1′ and 2-2′. The inverse Fourier transformation of the 1-1′ frequencies [Fig. 7(c)] suggests the presence of SiC crystallites (compare with Fig. 5(c)]. The transformation of the 2-2′ frequencies demonstrates the presence of long-period fringes with a distance of about 0.44 nm [Fig. 7(d)].

Normalized raw PEELS-spectra of the Cl–$L_{2,3}$ absorption edge of all samples are displayed in Fig. 8.

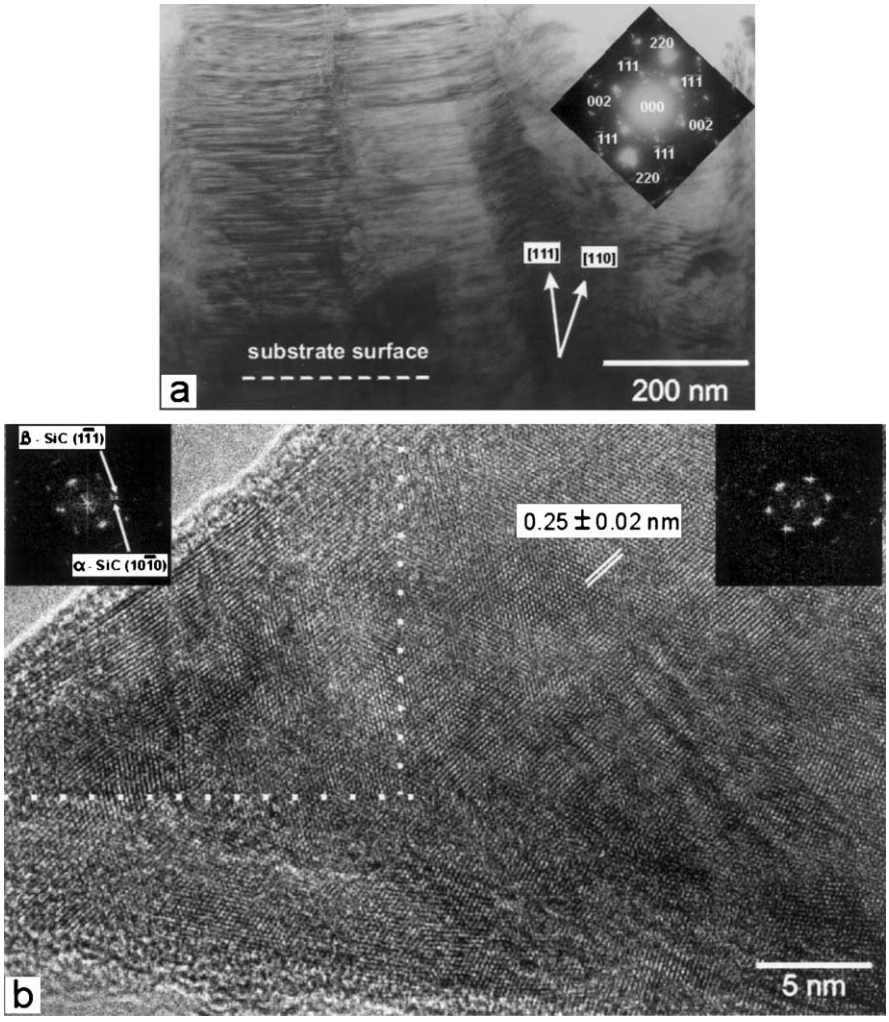

Fig. 2. Nanostructure of a sample deposited at 1100 °C. (a) Cross-sectional TEM image showing columnar crystallites of β-SiC exhibiting stacking-fault contrast; the white arrows show a faulted domain oriented perpendicular to the <111> direction and parallel to the substrate surface; the zone axis of diffraction pattern (inset) is close to the <110> direction. (b) HRTEM image and the corresponding FFT patterns (insets) of a thin crystallite; the FFT pattern placed on the left hand side was taken from the white dotted area and FFT pattern on the right hand was from the rest area of the image; the first FFT pattern contains reflections of two phases having the following homoepitaxial relationship: (0001) α-SiC // (110) β-SiC.

Chlorine is surprisingly detected in all samples, which covers a wide range of structures, highly textured at 1100 °C and nanocrystalline at 900 °C. Mechanical thinning and ion etching are not sufficient to remove chlorine. Even after a treatment at 1100 °C in flowing argon the chlorine signal intensity is clearly above the noise level as follows from a comparison with the spectrum of M-Bond 610 used for the cross-section specimen preparation. The presence of the sharp lines around 200 eV after annealing (Fig. 8, inset) is particularly noteworthy.

With all samples a typical delayed edge is observed where the maximum of energy loss for the Cl–$L_{2,3}$ appears about 15 eV beyond the start of the ionization edge.[20] This profile is a result of the effective centrifugal barrier when the final states show a quantum number of $l > 1$. The effect of annealing on the Cl–$L_{2,3}$ edge profile proves a change in the binding states of a Cl-containing phase. The appearance of the sharp "white line"—like peaks around 209 eV after annealing at 1100 °C (Fig. 8, inset) is related to transitions into unoccupied binding states.[22] This indicates a recrystallization of the Cl-containing phase.

4. Discussion

The investigation of samples deposited at 900, 1000 and 1100 °C by TEM, HRTEM and EFD show a clear influence of temperature. Pure crystalline SiC is deposited at 1100 °C (Fig. 2). It is composed of highly textured β-SiC with a small fraction of α-SiC. Similar textures of β-SiC and formation of α-SiC are reported in literature for deposits obtained in same temperature

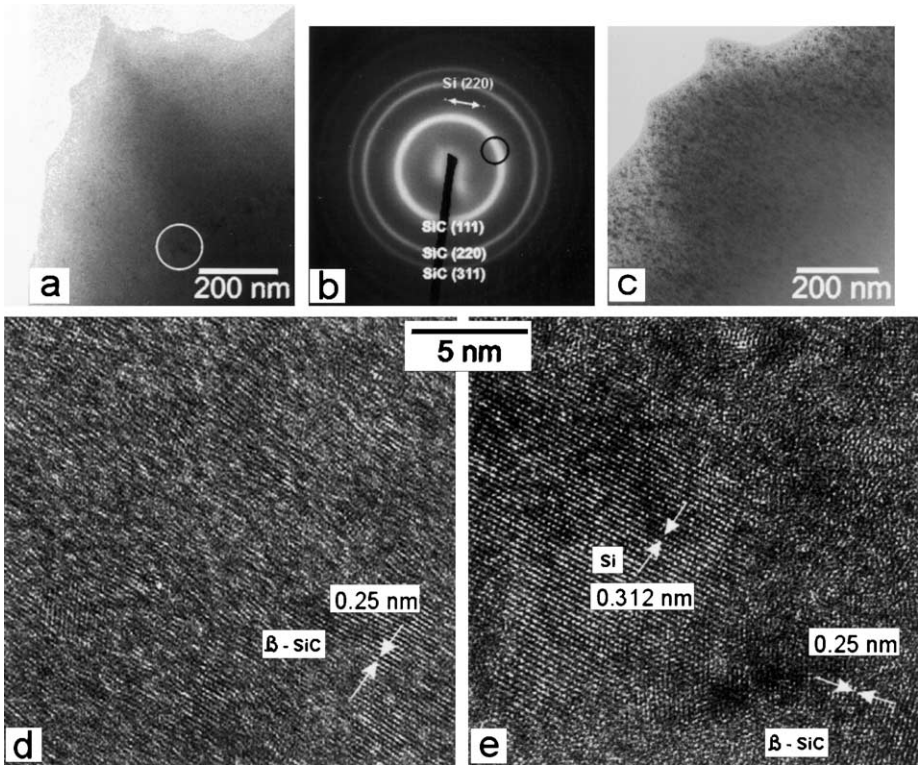

Fig. 3. Nanostructure of a sample deposited at 1000 °C. (a) Overview TEM image showing the β-SiC crystallite with Si inclusions (marked by a white circle). (b) Diffraction pattern containing diffuse rings of β-SiC and sharp dots of Si (marked by a double-sided arrow). (c) (111) Dark-field image demonstrating a relatively homogeneous distribution of β-SiC crystallite with an average size of about 5 nm. (d) HRTEM image showing a homogeneous distribution of the β-SiC crystallites. (e) HRTEM image of the area marked by the white circle showing a diffuse interphase region between the β-SiC and Si crystallites.

range.[2] Both SiC phases were also detected by X-ray diffraction[4,17,18] and Raman spectroscopy.[1,7] Formation of α-SiC is remarkable because the transformation temperature from β- to α-SiC is much higher than 1100 °C [13]. It is assumed that α-SiC is formed by a twinning transformation of heavily-faulted and deformed lamellae of β-SiC.[4,23] A similar explanation was employed to explain this transformation during sintering of β-SiC.[24,25]

At the lower temperatures α-SiC is not formed, but Si is co-deposited. Crystallite size and crystalline perfection of both, β-SiC and Si decrease with decreasing temperature. At 1000 °C the crystallites are separated by a less ordered interphase, which is mainly composed of SiC [Fig. 3(d) and (e)]. At 900 °C the crystallites are embedded in a disordered matrix composed of SiC and Si [Fig. 6(a)].

Co-deposition of Si at lower temperatures is well known.[2,7–9,26] More recent results on detailed structural analyses of deposits obtained at a very similar MTS/H_2 ratio and the same temperatures show similar tendencies as described above.[2] A direct comparison of the results is difficult because the geometry of the deposition space and the substrate as well as the residence time are not given. In particular, deposition rates can not be compared. One comparison, however, is necessary for discussion of deposition chemistry and kinetics. Pressures up to 20 kPa used in those studies are significantly lower than 90 kPa used in the present study. On the other hand, the (A/V) ratio may be estimated to be also significantly lower than 0.78 mm^{-1}. This implies a similar extent of gas phase reactions in both studies because a high ratio has a limiting effect on these reactions and thus compensates the effect of a high pressure.

This consideration may explain that heterogeneous deposits were also obtained in those earlier studies.[2] Deposition chemistry and kinetics as well as deposition models have to be discussed to demonstrate the significance of these observations with respect to the proposed deposition model.[17,18] In earlier models deposition of SiC as well as of Si are attributed to small species such as $SiCl_2$, $SiCl_3$, CH_3, CH_4, C_2H_4 and C_2H_2.[9–11,14] A carbosilane, $Cl_2Si=CH_2$, was discussed as an intermediate in a single paper [15], but shown not to be relevant.[17] According to these intermediates a growth mechanism based on separated reactions of Si and C precursors at the surface is postulated for SiC and Si deposition.[9,10,14] With such a model, deposition of obviously heterogeneous structures is difficult to explain, a surface diffusion of reactive intermediates [2] does not seem to be a strong argument. A mass transfer limitation at 1100 °C[2,9] is not a precondition for

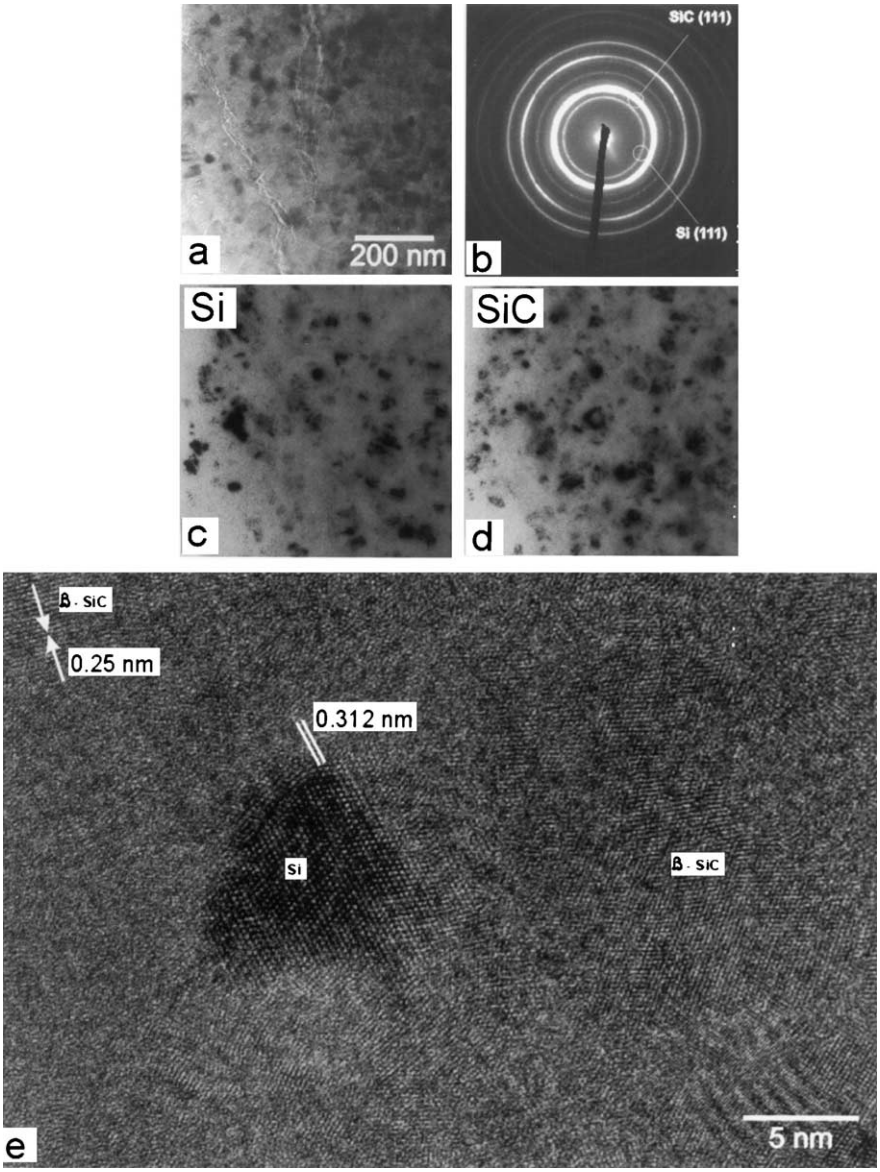

Fig. 4. Nanostructure of a sample deposited at 1000 °C and annealed at 1100 °C (40 h) in flowing argon. (a) Recrystallized grains appearing after annealing. (b) Diffraction pattern containing a set of sharp rings corresponding to β-SiC and Si phases. (c) and (d) Dark-field images obtained by selecting a part of the SiC (111) and Si (111) rings with the aid of objective aperture (shown by white circles in b). (e) HRTEM image showing a Si crystallite embedded in a matrix phase composing SiC crystallites. Note the presence of less crystallized transition layers between β-SiC and Si.

deposition of stoichiometric, crystalline SiC, as follows from the results of Ref. 16, partially presented in Fig. 1. They show a strong rate increase from 1000 to 1100 °C especially at the lower ratio of 0.78 mm^{-1}, at which the samples of the present study were prepared.

The proposed chemical model was developed to explain the unusual temperature dependency of the deposition rate,[16,17] which was observed by several authors,[9,26] but not explained. The above model is based on the assumption that higher carbochloro- and chlorosilanes are formed in gas phase reactions[17] as intermediates of SiC and Si deposition, respectively [Eqs. (1) and (2)]

$$n\ SiCl_2^{\bullet\bullet} \rightarrow \left\{ \begin{matrix} Cl \\ Si \\ Cl \end{matrix} \right\}_n \quad (1)$$

$$n\ ClSiCH_3^{\bullet\bullet} \rightarrow \left\{ \begin{matrix} CH_3 \\ Si \\ Cl \end{matrix} \right\}_n \rightarrow \left\{ \begin{matrix} H & H \\ Si & - & C \\ Cl & & H \end{matrix} \right\}_n \quad (2)$$

These intermediates are preferentially formed from $SiCl_2$ and CH_3. The pronounced temperature selectivity of deposition at 900 and 1025 °C [Fig. 1(a)] is attributed to different sources of $SiCl_2$.[17,18] An enhanced deposition of Si at lower temperatures results from a favored formation of higher chlorosilanes.

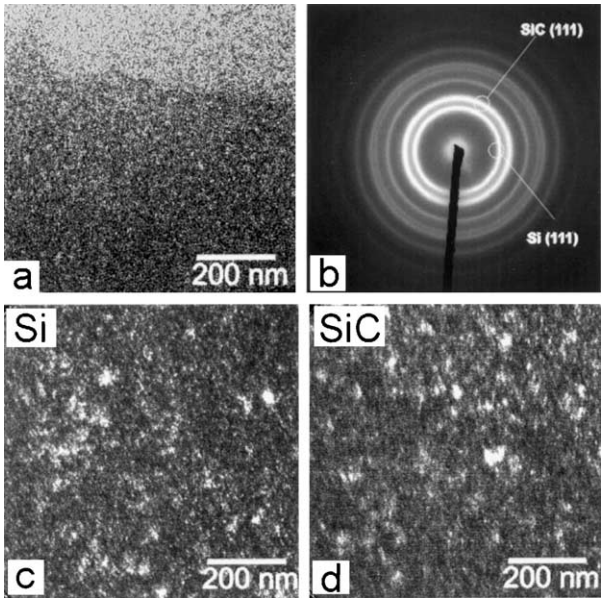

Fig. 5. Nanostructure of a sample deposited at 900 °C. (a) Low-resolution bright-field image exhibiting very low contrast. (b) Diffraction pattern with a set of diffuse β-SiC and Si reflections. (d) SiC (111)- and (c) Si (111)- dark-field images demonstrating a relatively homogeneous distribution of Si and β-SiC phases.

Formation of larger species leads to a supersaturation of the gas phase. Therefore, it is postulated that Si as well as SiC deposition are mainly based on a nucleation mechanism, at least at low (A/V) ratios, a well-known and very important mechanism of chemical vapor deposition of carbon.[27] Less pronounced gas phase reactions at a high (A/V) ratio may be recognized from the results of Fig. 1(b).

A nucleation mechanism seems to be more appropriate to understand deposition of heterogeneous structures, as shown in Figs. 3–7. Such a mechanism is supported by two additional results not reported before. A presence of chlorine in the bulk of the deposit implies a termination of Si surface atoms (Fig. 8). A further deposition should only be possible by a nucleation process. Detection of crystalline structures at 900 °C showing an interplanar distance similar to that of polychlorosilane, $[SiCl_2]_n$ (Fig. 9; *a-direction*),[28] and probably also to that of polycarbochlorosilane[29,30] is a further indication of a nucleation or condensation process.

In summary, it is concluded that the structural details of the deposits can satisfactorily be explained with the proposed chemical model, particularly if it is combined

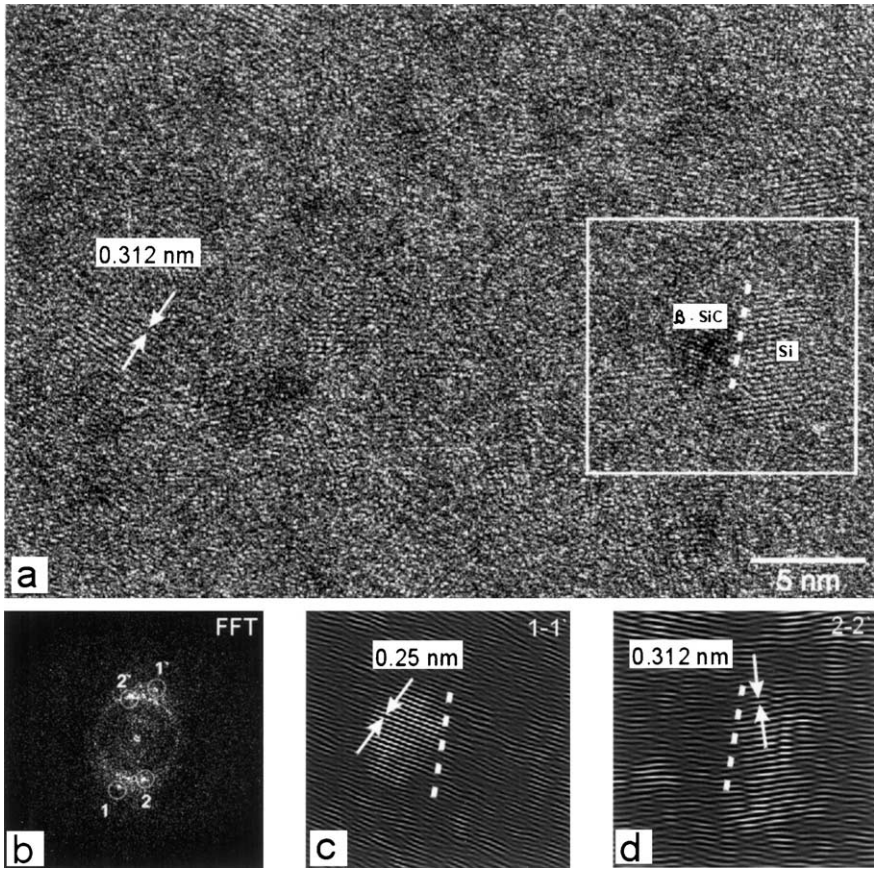

Fig. 6. HRTEM image of a sample deposited at 900 °C. Homogeneous distribution of β-SiC and Si crystallites with an average size of about 5 nm; the white square denotes the area analyzed by FFT. (b) FFT pattern with spatial frequencies (marked as 1-1′ and 2-2′) taken for image transformation. (c) (1-1′) FFT-1 pattern showing lattice fringes of β-SiC. (d) (2-2′) FFT-1 pattern showing lattice fringes of Si.

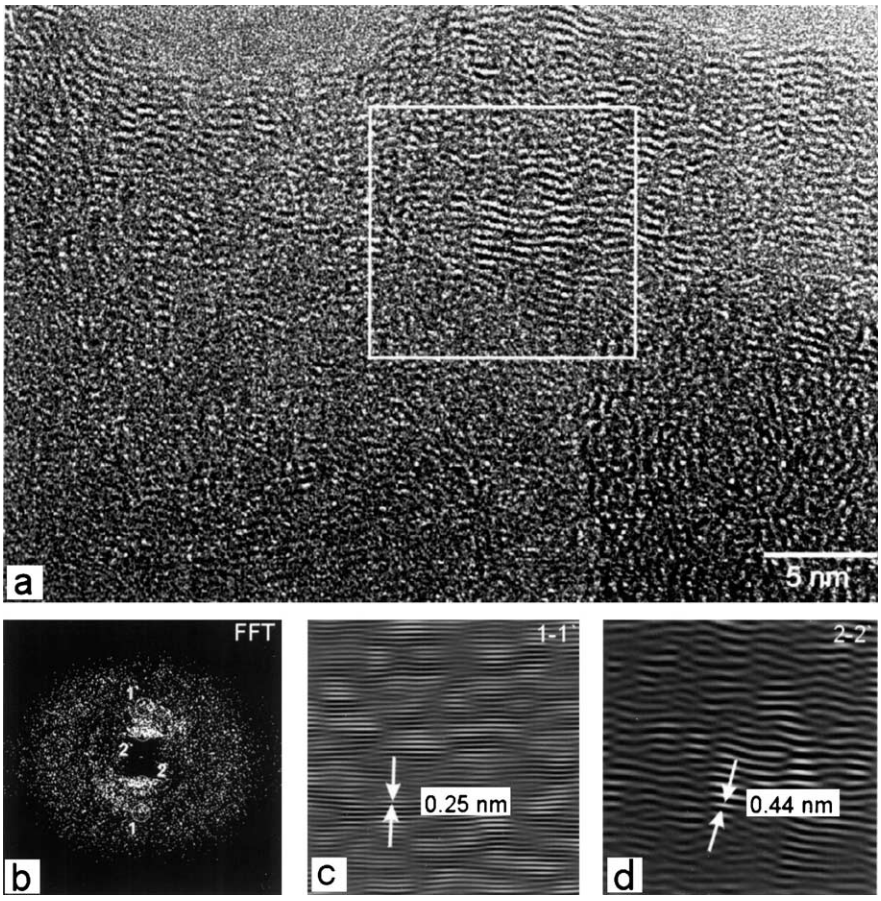

Fig. 7. HRTEM image of a sample deposited at 900 °C prepared as a powder. (a) Lattice fringes with a distance more than 0. 3 nm are frequently observed. (b) FFT pattern with spatial frequencies (marked as 1-1′ and 2-2′) taken for image transformation from the area marked by the white square. (c) (1-1′) FFT-1 pattern showing lattice fringes of β-SiC. (d) (2-2′) FFT-1 pattern showing fringes with the lattice distances of about 0. 44 nm.

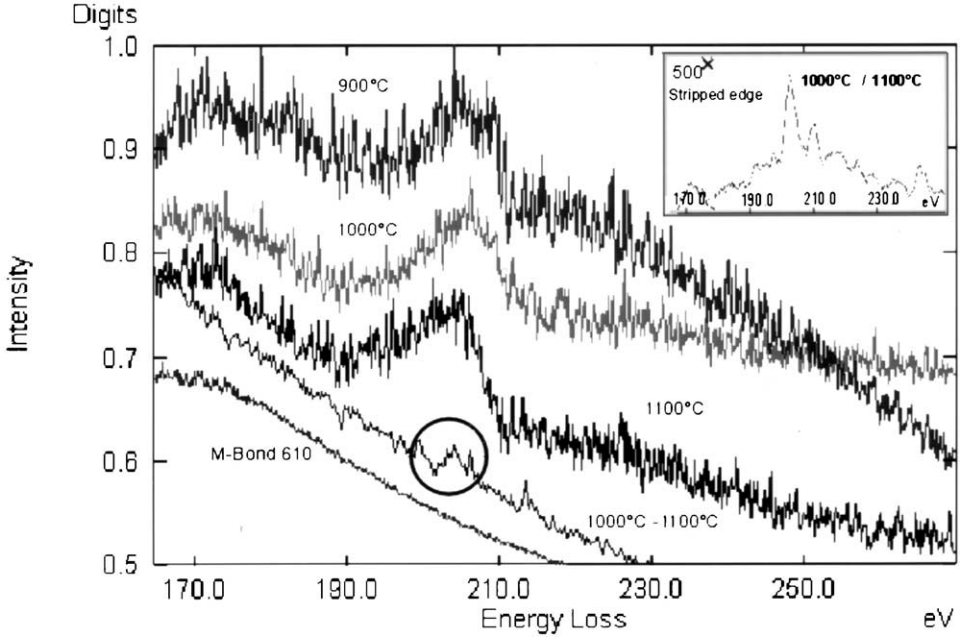

Fig. 8. Normalized raw PEELS-spectra of Cl-L2,3 absorption edge of deposits showing a chlorine signal in as deposited samples and its intensity decreasing after annealing; the area in the black circle is shown as an inset including the magnified spectrum after the background stripping using the power low function and noise reduction by smoothing. Note the sharp lines (transitions) around 209 eV in the enlarged spectrum.

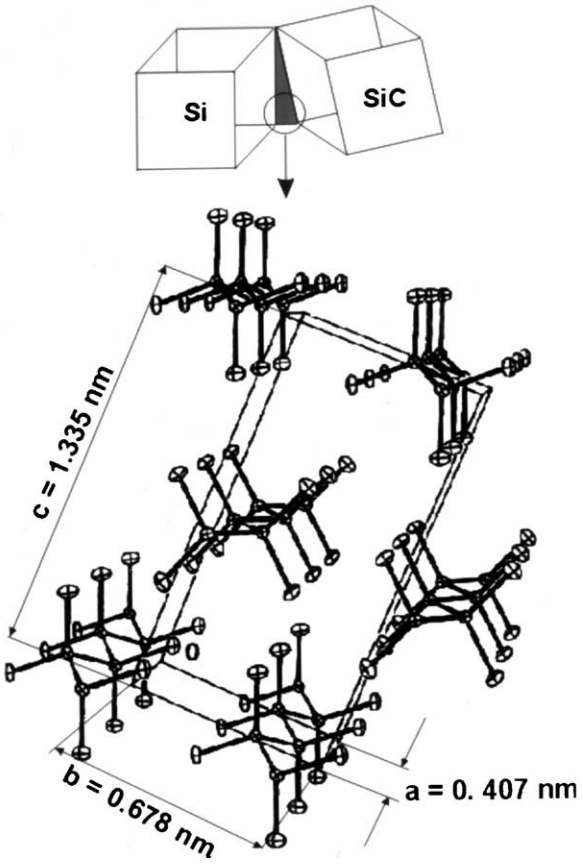

Fig. 9. Formation of tilted boundaries between Si and SiC crystallites due to the presence of the Cl-containing sheathing shell. The unit cell and molecular structure of the Cl shell is very close to $[SiCl_2]_n$, published by R. West and co-authors.[28]

with a nucleation mechanism of deposition. This does not exclude that a growth mechanism based on small species may be active at different deposition conditions, especially at very low pressures or very high (A/V) ratios.

Acknowledgements

Financial support of the study by the Deutsche Forschungsgemeinschaft (DFG) is gratefully acknowledged.

References

1. Stinton, D. P., Hembree, D. M., More, K. L., Sheldon, B. W., Besmann, T. M., Headinger, M. H. and Davis, R. F., Matrix characterization of fiber-reinforced SiC matrix composites fabricated by chemical vapor infiltration. *J. Mater. Sci.*, 1995, **30**, 4279–4285.
2. Loumagne, F., Langlais, F., Naslain, R., Schamm, S., Dorignac, D. and Sevely, J., Physicochemical properties of SiC-based ceramics deposited by low pressure chemical vapor deposition from CH_3SiCl_3–H_2. *Thin Solid Films*, 1995, **254**, 75–82.
3. Lespiaux, D., Langlais, F., Naslain, R., Schamm, S. and Sevely, J., Chlorine and oxygen inhibition effects in the deposition of SiC-based ceramics from the Si–C–H–Cl system. *J. Eur. Ceram. Soc.*, 1995, **15**(1), 81–88.
4. Kim, H. and Choi, D., Effect of diluent gases on growth behavior and characteristics of chemically vapor deposited silicon carbide films. *J. Am. Ceram. Soc.*, 1999, **82**(2), 331–337.
5. Papasouliotis, G. D. and Sotirchos, S. V., Hydrogen chloride effects on the CVD of silicon carbide from methyltrichlorosilane. *Adv. Mater.- CVD*, 1998, **4**(6), 235–246.
6. Martineau, P., Lahaye, M., Pailler, R., Naslain, R., Couzi, M. and Cruege, F., SiC filament/titanium matrix composites regarded as model composites. *J. Mater. Sci.*, 1984, **19**, 2731–2748.
7. Popovska, N., Held, D., Wunder, V., Gerhard, H. and Emig, G., Chemical vapor deposition of pyrolytical carbon and graded C/SiC/Si-films at atmospheric pressure. *Electrochem. Soc. Proc*, 1998, **23**, 407–412.
8. Josiek, A., Langlais, F. and Bourrat, X., A study of the transition between growth of stoichiometric and silicon-excess silicon carbide by CVD in the system MTS/H_2. *Adv. Mater.- CVD*, 1996, **2**(1), 17–21.
9. Langlais, F. and Prebende, C., On the chemical process of CVD of SiC-based ceramics from the Si–C–H–Cl system. *Proc. 11th Int. Conf. on CVD (Electrochem. Soc. Inc., Pennington, NJ)*, 1990, 686–695.
10. Loumagne, F., Langlais, F. and Naslain, R., Reaction mechanisms of the chemical vapor deposition of SiC-based ceramics from CH_3SiCl_3/H_2 gas precursor. *J. Crystal Growth*, 1995, **155**, 205–213.
11. Jonas, S., Ptak, W. S., Sadowski, W., Walasek, E. and Paluszkiewicz, C., FTIR in situ studies of the gas phase reactions in chemical vapor deposition of SiC. *J. Electrochem. Soc.*, 1995, **142**(7), 2357–2362.
12. Heuer, A. H., Fyburg, G. A., Ogbuji, L. U. and Mitchell, T. E., A transformation in polycrytsalline SiC: I, microstructural aspects. *J. Am. Ceram. Soc.*, 1978, **61**, 406–411.
13. Najajima Y. In *Silicon Carbide Ceramics-1, Fundamental and Solid Reaction*. ed. S. Somiya and Y. Inomata. Elsevier Applied Science, London and NewYork, 1991.
14. *Gmelin Handbook Silicon* B3, pp. 99–101.
15. Allendorf, M. D. and Melius, C. F., Theoretical study of the thermochemistry of molecules in the Si–C–Cl–H system. *J. Phys. Chem.*, 1993, **97**(3), 720–728.
16. Zhang, W. G. and Hüttinger, K. J., Chemical vapor deposition of SiC from methyltrichlorosilane. Part I: deposition rates. *Adv. Mater.- CVD*, 2001, **7**(4), 167–172.
17. Zhang, W. G. and Hüttinger, K. J., Chemical vapor deposition of SiC from methyltrichlorosilane. Part II: composition of the gas phase and the deposit. *Adv. Mater.- CVD*, 2001, **7**(4), 173–181.
18. Zhang, W. G. and Hüttinger, K. J., Chemical vapor deposition of silicon carbide at various temperatures and surface area/volume ratios. *J. Phys. IV France*, 2001, **11**(3), 55–61.
19. Hüttinger, K. J., CVD in hot wall reactors—the interaction between homogeneous gas-phase and heterogeneous surface reactions. *Adv. Mater.- CVD*, 1998, **4**(4), 151–158.
20. Hu, Z. and Hüttinger, K. J., About the determination of kinetics of CVD in hot wall reactors. *Adv. Mater.- CVD*, 2000, **6**(2), 77–82.
21. Williams, D. B., Practical analytical electron microscopy in materials science. *Chemie international*, 1984.
22. Reimer, L., *Scanning Electron Microscopy*. Springer Verlag, Berlin, 1985.
23. Gulden, T. D., Deposition and microstructure of vapor-deposited silicon carbide. *J. Am. Ceram. Soc.*, 1968, **51**(8), 424–427.
24. Ogbuji, L. U., Mitchel, T. E. and Heuer, A. H., A transformation in polycrytsalline SiC: III, the thickening of a plates. *J. Am. Ceram. Soc.*, 1978, **61**, 91.
25. Mitchel, T. E., Ogbuji, L. U. and Heuer, A. H., A transformation in polycrytsalline SiC: II, interfacial energetics. *J. Am. Ceram. Soc.*, 1978, **61**, 412.

26. Papasouliotis, G. D. and Sotirchos, S. V., On the homogeneous chemistry of the thermal decomposition of methyltrichlorosilane. *J. Electrochem. Soc*., 1994, **141**(6), 1599–1610.
27. Hu, Z. J. and Hüttinger, K. J., Mechanisms of carbon deposition—a kinetic approach. *Carbon*, 2002, **40**(4), 624–628.
28. Koe, J. R., Powell, D. R., Buffy, J. J., Hayase, S. and West, R., Perchloropolysilane: X-ray structure, solid-state ^{29}Si NMR spectroscopy, and reactions of $(SiCl_2)_n$. *Angew. Chem., Int. Ed*., 1998, **37**(10), 1441–1442.
29. Wu, H. J. and Interrante, L. V., Preparation of poly(dichlorosilaethylene) and poly(silaethylene) via ring-open polymerization. *Macromolecules*, 1992, **25**(6), 1840–1841.
30. Interrante, L. V. and Shen, Q. H. Polycarbosilanes. In *Silicon-containing Polymers*. Kluwer Acdemic Pubs.; 2000, 244–321.